Preclinical Evaluation of $^{203/212}$Pb-Labeled Low-Molecular-Weight Compounds for Targeted Radiopharmaceutical Therapy of Prostate Cancer

Sangeeta Ray Banerjee[1,2], Il Minn[1], Vivek Kumar[1], Anders Josefsson[1], Ala Lisok[1], Mary Brummet[1], Jian Chen[1], Ana P. Kiess[2], Kwamena Baidoo[3], Cory Brayton[4], Ronnie C. Mease[1,2], Martin Brechbiel[3], George Sgouros[1], Robert F. Hobbs[1], and Martin G. Pomper[1,2]

[1]Russell H. Morgan Department of Radiology and Radiological Science, Johns Hopkins University School of Medicine, Baltimore, Maryland; [2]Sidney Kimmel Comprehensive Cancer Center, Johns Hopkins University School of Medicine, Baltimore, Maryland; [3]National Institutes of Health, Bethesda, Maryland; and [4]Department of Pathology, Johns Hopkins University School of Medicine, Baltimore, Maryland

Targeted radiopharmaceutical therapy (TRT) using α-particle radiation is a promising approach for treating both large and micrometastatic lesions. We developed prostate-specific membrane antigen (PSMA)–targeted low-molecular-weight agents for ^{212}Pb-based TRT of patients with prostate cancer (PC) by evaluating the matching γ-emitting surrogate, ^{203}Pb. **Methods:** Five rationally designed low-molecular-weight ligands (L1-L5) were synthesized using the lysine-urea-glutamate scaffold, and PSMA inhibition constants were determined. Tissue biodistribution and SPECT/CT imaging of ^{203}Pb-L1–^{203}Pb-L5 were performed on mice bearing PSMA(+) PC3 PIP and PSMA(−) PC3 flu flank xenografts. The absorbed radiation dose of the corresponding ^{212}Pb-labeled analogs was determined using the biodistribution data. Antitumor efficacy of ^{212}Pb-L2 was evaluated in PSMA(+) PC3 PIP and PSMA(−) PC3 flu tumor models and in the PSMA(+) luciferase-expressing micrometastatic model. ^{212}Pb-L2 was also evaluated for dose-escalated, long-term toxicity. **Results:** All new ligands were obtained in high yield and purity. PSMA inhibitory activities ranged from 0.10 to 17 nM. ^{203}Pb-L1–^{203}Pb-L5 were synthesized in high radiochemical yield and specific activity. Whole-body clearance of ^{203}Pb-L1–^{203}Pb-L5 was fast. The absorbed dose coefficients (mGy/kBq) of the tumor and kidneys were highest for ^{203}Pb-L5 (31.0, 15.2) and lowest for ^{203}Pb-L2 (8.0, 4.2). The tumor-to-kidney absorbed dose ratio was higher for ^{203}Pb-L3 (3.2) and ^{203}Pb-L4 (3.6) than for the other agents, but with lower tumor-to-blood ratios. PSMA(+) tumor lesions were visualized through SPECT/CT as early as 0.5 h after injection. A proof-of-concept therapy study with a single administration of ^{212}Pb-L2 demonstrated dose-dependent inhibition of tumor growth in the PSMA(+) flank tumor model. ^{212}Pb-L2 also demonstrated an increased survival benefit in the micrometastatic model compared with ^{177}Lu-PSMA-617. Long-term toxicity studies in healthy, immunocompetent CD-1 mice revealed kidney as the dose-limiting organ. **Conclusion:** ^{203}Pb-L1–^{203}Pb-L5 demonstrated favorable pharmacokinetics for ^{212}Pb-based TRT. The antitumor efficacy of ^{212}Pb-L2 supports the corresponding ^{203}Pb/^{212}Pb theranostic pair for PSMA-based α-particle TRT in advanced PC.

Key Words: α-particle; theranostic pair; prostate-specific membrane antigen; murine pharmacokinetics; lead-212

J Nucl Med 2020; 61:80–88
DOI: 10.2967/jnumed.119.229393

Targeted radiopharmaceutical therapy using α-particles (α-TRTs), which cause deposition of ionizing radiation of high-linear-energy transfer, is accelerating in importance for managing prostate cancer (PC). This acceleration is due in part to the unexpected survival benefit conferred by $^{223}RaCl_2$ in patients with castration-resistant PC metastatic to bone (*1*). Also contributing to this acceleration has been the remarkable decrease in tumor burden demonstrated on images of patients who received ^{225}Ac-PSMA-617 (*2*), which targets prostate-specific membrane antigen (PSMA) in patients with metastatic castration-resistant PC who failed prior standard treatment (*3,4*). However, salivary and lacrimal gland radiotoxicity may affect the overall survival benefit by reducing quality of life (*5*). As an alternative to ^{225}Ac (half-life, 10 d), ^{212}Pb, which has a shorter physical half-life (10.6 h), is a promising source of α-emissions that has proved safe and effective in both preclinical models and clinical studies for several indications (*6–9*). ^{212}Pb is commercially available from a ^{224}Ra generator and has well-described radiochemistry (*10*). It is a β-emitter but serves as an in vivo nanogenerator of ^{212}Bi (half-life, 1.01 h), which decays with an α-particle in its decay chain. ^{212}Pb has been successfully used as a stand-alone treatment and in combination with chemotherapy using peptides and monoclonal antibodies as targeting vectors (*6,7,11*). Although PSMA-based TRT using low-molecular-weight agents and monoclonal antibodies is expanding in management of metastatic castration-resistant PC, to date this has primarily used agents that deliver β-emitting payloads (*12,13*). Few preclinical studies describe detailed evaluation of α-TRT (*14–17*).

A challenge of α-TRT is that the administered therapeutic activities are generally insufficient to be imaged for patient-specific dosimetry. For ^{212}Pb, preclinical evaluation presents additional challenges due to a high-energy γ-emission from a daughter that requires extra shielding. As a surrogate radionuclide, ^{203}Pb (half-life, 51.9 h, γ = 279 keV) is suitable for γ-well counting and SPECT and has been explored to aid development of ^{212}Pb-based

Received Apr. 4, 2019; revision accepted Jun. 18, 2019.
For correspondence or reprints contact: Sangeeta Ray Banerjee, Johns Hopkins University School of Medicine, 1550 Orleans St., CRBII, Room 4M 07, Baltimore, MD 21287.
E-mail: sray9@jhmi.edu
Published online Jun. 28, 2019.

α-TRT (*18,19*). A first-in-humans study using ^{203}Pb-based PSMA SPECT has recently appeared (*20*).

Here we report preclinical evaluation of a series of ^{203}Pb-labeled low-molecular-weight ligands (L1–L5) for PSMA α-TRT. We first reevaluated our previous lead agent, L1 (*21*), as the ^{203}Pb-labeled analog, and then synthesized 4 new ligands L2–L5 with further alterations to the chelator and inclusion of a 4-bromobenzyl-lysine-urea-glutamate targeting moiety. We used the 4-bromobenzyl derivative of lysine-urea-glutamate as the targeting moiety because of the sustained tumor uptake and high efficacy previously demonstrated by ^{125}I-DCIBzL and its short-half-life α-emitting analog, ^{211}At-6 (half-life, 7.2 h) (*15,22*) (Fig. 1). The goal of this study was to optimize an α-emitting agent with decreased off-target radiotoxicity relative to ^{211}At-6 for PSMA-based α-TRT.

MATERIALS AND METHODS

Reagents, Cell Lines, and Animal Models

^{203}Pb was produced at the NIH Clinical Center cyclotron facility using a ^{203}Tl(d,n)/^{203}Pb reaction and purified from the target as previously described (*23*). The ^{212}Pb was obtained using a ^{224}Ra/^{212}Pb generator (Oak Ridge National Laboratories). Sublines of the androgen-independent PC3 human PC cell line, originally derived from an advanced androgen-independent bone metastasis, were used (*24*). Animal studies were in compliance with the regulations of the Johns Hopkins Animal Care and Use Committee. Six- to 8-wk-old male nonobese, diabetic/Shi-scid/IL-2rgnull (NSG; The Jackson Laboratory) mice (Johns Hopkins Animal Resources Core) were implanted subcutaneously with PSMA(+) PC3 PIP (1.5×10^6) cells and PSMA(−) PC3 flu cells (1×10^6) in the forward right and left flanks, respectively.

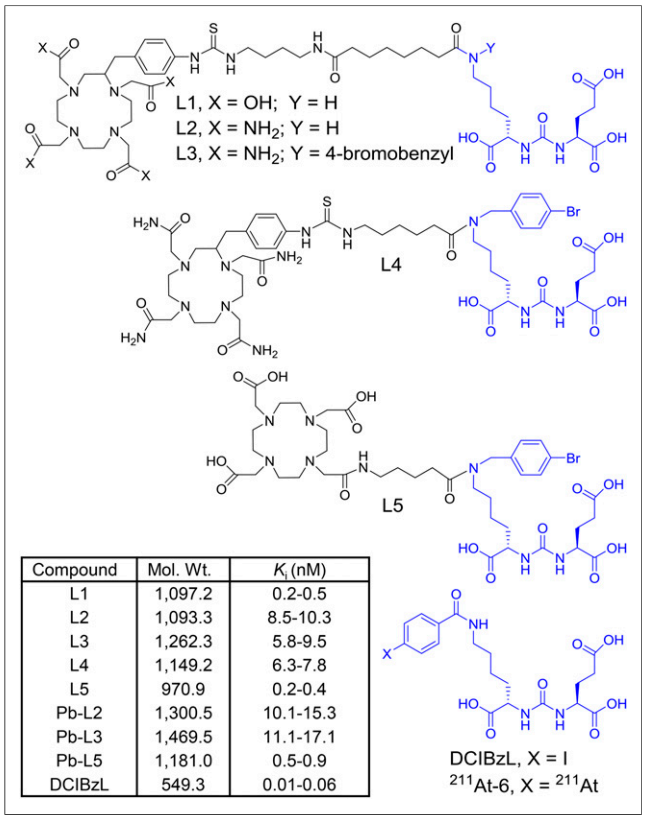

Compound	Mol. Wt.	K_i (nM)
L1	1,097.2	0.2-0.5
L2	1,093.3	8.5-10.3
L3	1,262.3	5.8-9.5
L4	1,149.2	6.3-7.8
L5	970.9	0.2-0.4
Pb-L2	1,300.5	10.1-15.3
Pb-L3	1,469.5	11.1-17.1
Pb-L5	1,181.0	0.5-0.9
DCIBzL	549.3	0.01-0.06

FIGURE 1. Structures of DCIBzL, ^{211}At-6, and ligands L1–L5, for $^{203/212}$Pb-labeled PSMA-targeted α-particle theranostics. Molecular weight and PSMA inhibition constant (K_i) of new compounds are listed in the inset table.

Chemistry

Ligands L1 (*21*) and L5 (*25*) and intermediates 3 (*24*) and 4 (*25*) were synthesized following our recent reports. Detailed descriptions for L2, L3 (*26*), L4, and L5 are provided in the supplemental data (available at http://jnm.snmjournals.org). The PSMA binding affinity of the new compounds was determined using a fluorescence-based competitive binding assay reported by our laboratory (*15*).

Radiolabeling

An acidic solution of $^{203}PbCl_2$ (~25.9 MBq in 100 μL) was neutralized with 6 μL of 5 M NH_4OAc to obtain a pH of approximately 4.5–5.5. A solution (40 μL) of L1–L5 (1 mg/800 μL of 0.1N H_4OAc) was added, and the reaction mixture was incubated at 60°C–65°C for 45 min. An identical procedure was followed for radiosynthesis of each ^{203}Pb-labeled analog. Radiolabeling was nearly quantitative in each case. ^{212}Pb-L2 was synthesized following a literature method (*27*) at the National Cancer Institute and transported to Johns Hopkins for treatment studies.

Biodistribution

Mice bearing PSMA(+) PC3 PIP and PSMA(−) PC3 flu xenografts were injected via the tail vein with approximately 1.85 MBq of ^{203}Pb-L1-^{203}Pb-L5 ($n = 4$). Competitive inhibition studies were performed using ZJ43 (*28*), a known low-molecular-weight PSMA inhibitor, added to the ^{203}Pb-L2–^{203}Pb-L5 formulation, and biodistribution studies were performed at 2 h ($n = 4$).

SPECT/CT Imaging

SPECT/CT imaging of ^{203}Pb-L1, ^{203}Pb-L2, ^{203}Pb-L3, and ^{203}Pb-L4 was performed on an X-SPECT device (GammaMedica) following a reported method (*24*). Data were reconstructed and fused using commercial software from the vendor. Data were analyzed using AMIRA software (Thermo Fisher Scientific).

Dosimetry

Time–activity curves were generated from the murine biodistribution data of the ^{203}Pb-analogs. Normal tissue and tumor absorbed-dose coefficients (ADCs) were estimated for the ^{212}Pb-labeled analog after accounting for the α-radiation deposited locally using the mathematic formalism established by MIRD (*29*). Only the α-emission was considered in the calculations and was assumed to be deposited locally ($\varphi = 1$). Selected human ADCs were estimated using a mouse-to-human conversion formula for time-integrated activities, which were then input into OLINDA/EXM (*30*).

The preclinical biodistribution data (percentage injected dose [%ID] per gram of tissue) were translated into human whole-organ biodistribution data (%ID/organ) based on the ratio of organ activity concentration to whole-body mass being equal in both species.

$$\left[\frac{\%ID}{organ}\right]_H = \left[\frac{\%ID}{g}\right]_M \cdot TBW_M \cdot \frac{OW_H}{TBW_H}, \qquad \text{Eq. 1}$$

where *M* is mouse, *H* is human, TBW is total body weight (25 g for a mouse and 73.7 kg for an adult male human), and OW is the average male organ weight, in kilograms. The time-integrated activity coefficients were calculated for the human adult male organs and used as input into OLINDA/EXM, version 1.0, to calculate the clinical ADCs. For the tumor calculations, the OLINDA/EXM version 1 sphere model was used for a 1 g sphere (*30*).

Radiopharmaceutical Therapy with ^{212}Pb-L2

Therapy in the Xenograft and Micrometastatic Models. Mice were injected subcutaneously in the upper flank with PSMA(+) PC3 PIP or

PSMA(−) PC3 flu cells. Treatments were administered when tumor volume was 60–100 mm^3. Animals (n = 5/group) received a single dose of 1.5 and 3.7 MBq of ^{212}Pb-L2 intravenously via tail-vein injection or were untreated. Tumors were then measured 2–3 times per week until they reached a volume that was 10-fold the initial volume. The probability of reaching 10 times the initial tumor volume was characterized using Kaplan–Meier curves, and a comparison was performed using the log-rank test. For the PSMA(+) micrometastatic model, mice were injected intravenously with 1×10^6 PC3-ML-Luc-PSMA cells, as previously reported by us (*15*). At 24 h after injection of the tumor cells, mice (n = 5/group) were injected intravenously with 0, 0.7, 1.5, and 3.7 MBq of ^{212}Pb-L2 and 37 MBq of ^{177}Lu-PSMA-617. Metastatic tumor progression and survival were monitored by in vivo bioluminescence imaging (IVIS Spectrum; Perkin-Elmer).

Determination of Maximum Tolerated Dose (MTD). The MTD was defined as the highest dose at which no animal died or lost more than 20% of its pretreatment weight. Non–tumor-bearing CD-1 mice (Charles River, n = 5/group) received intravenous injections of ^{212}Pb-L2 and were then weighed and inspected twice per week for at least 12 mo. Urinalysis was performed monthly. On sacrifice, animals were evaluated at the Johns Hopkins Phenotyping Core, which obtained a serum metabolic panel, blood counts, and full necropsy.

Statistical Analysis

Statistical analysis was performed using a 2-tailed t test (GraphPad). P values were considered significant at a level of 0.05.

RESULTS

Synthesis and Radiolabeling

An abbreviated structure–activity relationship study was performed by modifying the chelating agent, linker, and targeting scaffold to develop an optimized agent for α-TRT (Fig. 1). Ligands L1 and L2 were synthesized following our previous report (Supplemental Fig. 1A) (*21*). Although DOTA-monoamide was successfully used for a ^{212}Pb-labeled peptide (*6*), considering the unusual stability of Pb-(1,4,7,10-tetra-(2-carbamoyl methyl)-cyclododecane (TCMC) compounds in an acidic environment (*11,31*), L2–L4 were designed to contain a TCMC chelating agent. L3–L5 were synthesized following a similar route using the 4-bromobenzyl derivative of the Glu-urea-Lys scaffold (Supplemental Figs. 2B and 2C). ^{203}Pb-labeled compounds (^{203}Pb-L1–^{203}Pb-L5) and ^{212}Pb-L2 were synthesized in greater than 95% yield and were separated from the corresponding nonradiolabeled precursor by high-performance liquid chromatography to obtain a pure product with a specific activity of 0.7–1.9 MBq/nmol. The stability of the radiolabeled compounds was determined by incubation in phosphate-buffered saline and in 0.1% human serum albumin in phosphate-buffered saline (×1) at 37°C up to 72 h and was greater than 95%.

In Vivo Evaluation

Tissue Biodistribution. Biodistribution data (expressed in %ID/g) of ^{203}Pb-L1–^{203}Pb-L5 are shown in Figure 2 and Supplemental Tables 1–5. ^{203}Pb-L1 exhibited high uptake in the PSMA(+) PC3 PIP tumor as early as 1 h, remained high at 4 h, and decreased at 24 h after injection. Unlike ^{203}Pb-L1, ^{203}Pb-L2 demonstrated the highest uptake in the PSMA(+) tumor at 2 h, followed by gradual clearance during 4–24 h after injection. ^{203}Pb-L2 displayed fast clearance from all normal tissues including kidneys and PSMA(+) tumor. Observing the significant change in biodistribution, especially within the PSMA(+) PC3 PIP tumor and the kidneys by simply changing the chelating agent as we previously experienced (*32*), we further investigated radioligands ^{203}Pb-L3 and ^{203}Pb-L4 bearing the same chelating agent, TCMC-Bn-NCS, and ^{203}Pb-L5 bearing the DOTA-monoamide chelating agent. Figure 3 summarizes the head-to-head comparison of the PSMA(+) tumor and selected tissues of the tested agents. ^{203}Pb-L2 demonstrated significantly lower tumor uptake up to 2 h than ^{203}Pb-L1, ^{203}Pb-L3, and ^{203}Pb-L5 ($P <$ 0.01). At 4 h, ^{203}Pb-L2 displayed significantly lower tumor uptake than any other compound (^{203}Pb-L1 and ^{203}Pb-L4, $P < 0.001$; ^{203}Pb-L3 and ^{203}Pb-L5, $P < 0.05$). Additionally, at 24 h after injection, tumor uptake of ^{203}Pb-L2 was significantly lower than that of ^{203}Pb-L1, ^{203}Pb-L3, and ^{203}Pb-L5. There was no significant difference in PSMA(+) tumor uptake between ^{203}Pb-L3 and ^{203}Pb-L4 during the 0.5- to 24-h time-points. Both ^{203}Pb-L1 and ^{203}Pb-L5 showed significantly higher tumor retention than ^{203}Pb-L3 at 24 h.

^{203}Pb-L2–^{203}Pb-L4 with the TCMC chelating agent displayed significantly lower renal uptake during 1–4 h after injection than ^{203}Pb-L1 and ^{203}Pb-L5. At 24 h, renal uptake was significantly lower for ^{203}Pb-L2–^{203}Pb-L4 than for ^{203}Pb-L1 ($P < 0.001$). ^{203}Pb-L5 displayed significantly higher renal uptake at 2 h and remained high compared with ^{203}Pb-L1 during 4–24 h. There was no significant difference in renal uptake between

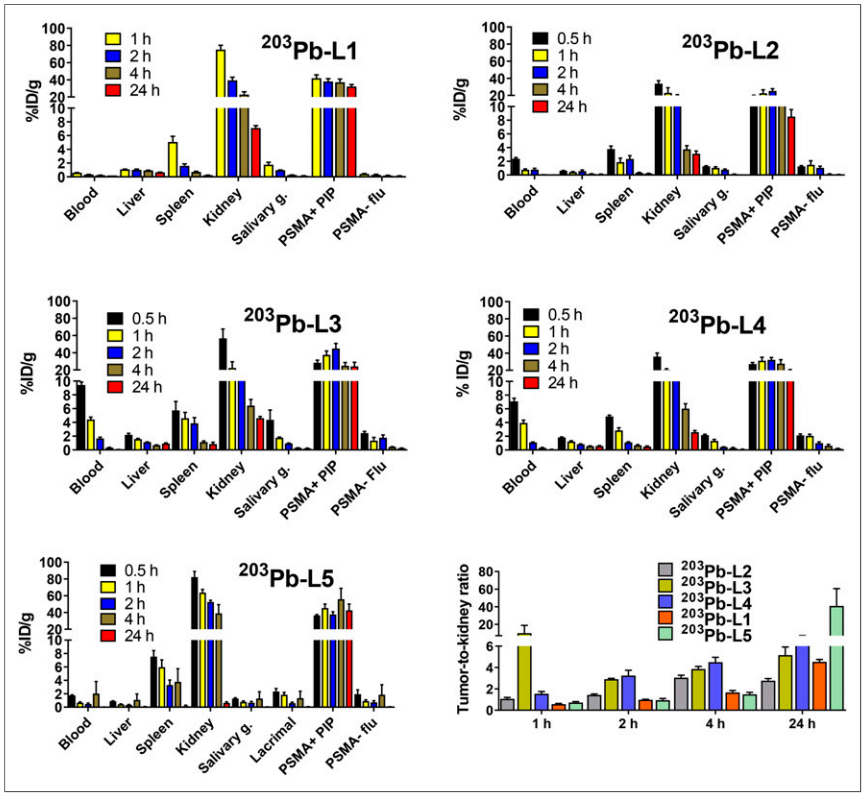

FIGURE 2. Tissue biodistribution in mice bearing PSMA(+) PC3 PIP and PSMA(−) PC3 flu tumors on either flank (n = 4) and tumor–to–normal-organ ratios.

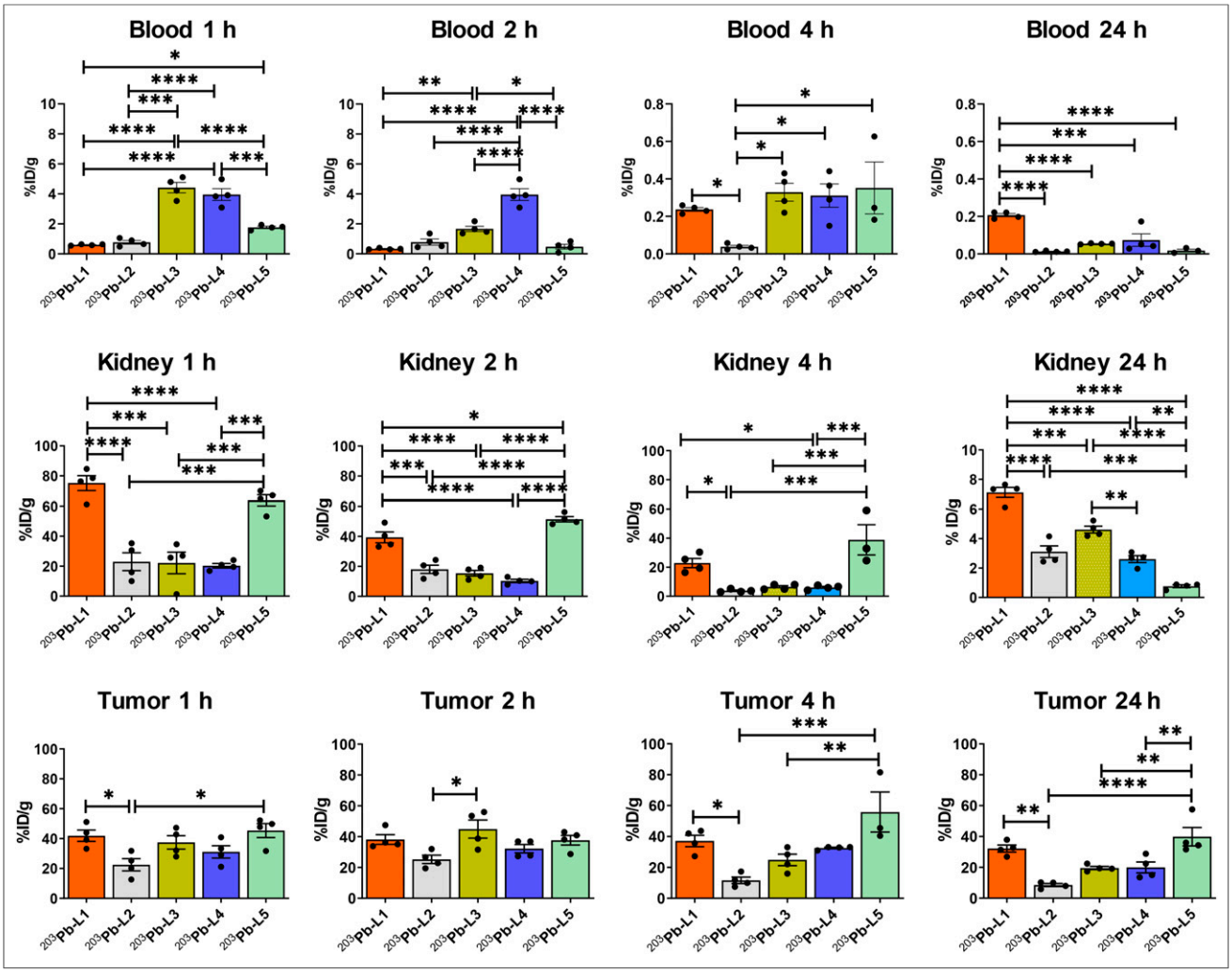

FIGURE 3. Time-dependent uptake of ^{203}Pb-L1–^{203}Pb-L5 in selected tissues. *$P < 0.05$. **$P < 0.01$. ***$P < 0.001$. ****$P < 0.0001$.

^{203}Pb-L2, ^{203}Pb-L3, and ^{203}Pb-L4 up to 4 h and a small but significant difference at 24 h only between ^{203}Pb-L2 and ^{203}Pb-L3. Blocking (PSMA binding specificity) studies were performed for ^{203}Pb-L2–^{203}Pb-L5 by coadministration of 50–100 nmol of the known PSMA inhibitor, ZJ43 (*28*), showing significant blockade in the PSMA(+) PC3 PIP tumor for all agents (Supplemental Fig. 2). Significant renal blockade was observed for all agents, further indicating specificity for PSMA.

Organ-Absorbed Doses. Figure 4 and Supplemental Table 6 provide a selected list of the murine ADC for ^{212}Pb-analogs. Tumors received ADCs of 23.1, 8.0, 18.3, 15.0, and 31.0 mGy/kBq for ^{212}Pb-L1, ^{212}Pb-L2, ^{212}Pb-L3, ^{212}Pb-L4, and ^{212}Pb-L5, respectively. Kidneys received the highest ADC and followed a similar trend to that of the PSMA(+) tumors, with 23.1, 4.4, 5.8, 4.1, and 15.2 mGy/kBq for ^{212}Pb-L1, ^{212}Pb-L2, ^{212}Pb-L3, ^{212}Pb-L4, and ^{212}Pb-L5, respectively. The other potential dose-limiting organ was blood, which demonstrated a nearly 2-fold higher ADC for ^{212}Pb-L3 (0.5 mGy/kBq) and ^{212}Pb-L4 (0.4 mGy/kBq) than for ^{212}Pb-L1 (0.2 mGy/kBq) and ^{212}Pb-L2 (0.1 mGy/kBq). Absorbed doses for other tissues were low, including heart, lung, liver, spleen, and muscle. Salivary gland ADCs were low, within the range of 0.28–0.35 mGy/kBq for all agents. Therapeutic PSMA(+) tumor–to–normal-organ ratios were calculated for kidney, blood, and salivary glands (Fig. 5 inset). Therapeutic ratios with respect to kidney demonstrated the following trend: ^{212}Pb-L3 > ^{212}Pb-L4 > ^{212}Pb-L5 > ^{212}Pb-L1 ~ ^{212}Pb-L2. With respect to blood, the trend was ^{212}Pb-L1 > ^{212}Pb-L5 > ^{212}Pb-L4 > ^{212}Pb-L3 ~ ^{212}Pb-L2. Therapeutic ratios with respect to salivary glands were in the range of blood, indicating kidney as the dose-limiting organ. Estimated human ADCs from OLINDA/EXM, based on mouse-to-human time-integrated activity conversion, are listed in Supplemental Table 7.

In Vivo Imaging. SPECT/CT imaging was performed for ^{203}Pb-L1–Pb-L4 for a visual demonstration of in vivo pharmacokinetics (Fig. 5). SPECT/CT images during 0.5–24 h after administration confirmed high uptake in the PSMA(+) PC3 PIP tumors but not in the PSMA(−) PC3 flu tumors. Also consistent with the biodistribution data, ^{203}Pb-L2, ^{203}Pb-L3, and ^{203}Pb-L4 displayed very low renal uptake compared with ^{203}Pb-L1 at 2 h after injection. Fast blood clearance of all agents was also evident from the imaging study. Compared with ^{203}Pb-L4 (short linker), ^{203}Pb-L3, which bears a long linker, displayed high spleen uptake up to 4 h.

Radiopharmaceutical Therapy

Antitumor Effect in the Flank Tumor Model. The treatment effects of ^{212}Pb-L2 on the tumor growth rate and body weight of

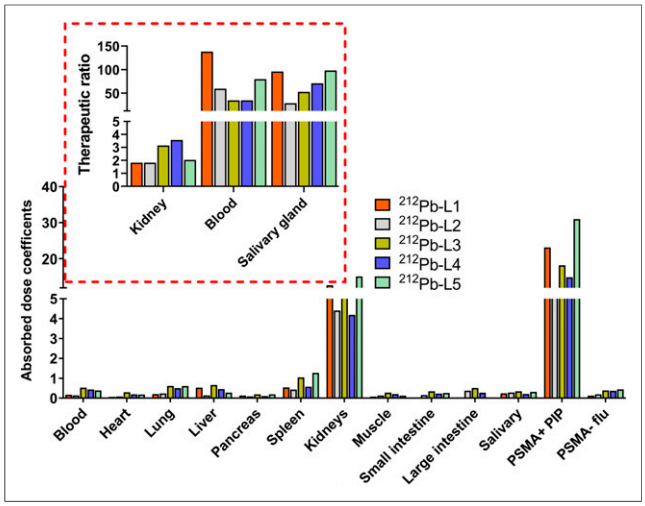

FIGURE 4. Estimated ADCs (mGy/kBq). Inset shows therapeutic ratio, calculated as ADCs of tumor-to-blood (Blood), tumor-to-kidney (Kidney), and tumor-to-salivary glands (Salivary gland).

the mice are shown in Figures 6A–6B. A single administration of 1.5 or 3.7 MBq showed significant tumor growth delay only in PSMA(+) tumors ($P = 0.003$), compared with the other groups; however, slow tumor regrowth was observed after 8 wk. The median time to reach a 10-fold increase from the initial tumor volume (tumor volume/initial volume ≤ 10) was 25 and 39 d for the treatment groups bearing PSMA(+) tumors administered 1.5 and 3.7 MBq, respectively (Fig. 6C). For control groups, untreated PSMA(+) and PSMA(−) tumors reached a 10-fold increase from the initial tumor volume at 13 and 15 d, respectively. The median time for a 10-fold tumor increase in the groups with PSMA(−) tumors treated with 1.5 and 3.7 MBq were 7.5 and 16 d.

Antitumor Effect in the PSMA(+) Micrometastatic Model. For the PSMA(+) micrometastatic tumor model, doses were administered 24 h after tumor cell inoculation. At that time, tumors were considered to be clusters of relatively few cells, which should be favorable for the short range of α-particles, compared with long-range β^--TRT. The efficacy of α-particle–emitting ^{212}Pb-L2 (single administration of 0.7, 1.5, and 3.7 MBq) was compared with an untreated group and a group treated with β-emitting ^{177}Lu-PSMA-617 (37 MBq) (Fig. 6D). No survival benefit was seen for the group treated with ^{177}Lu-PSMA-617 compared with the control group (median survival time, 46 and 47 d, respectively); in contrast, the median survival time for the mice administered ^{212}Pb-L2 (3.7 MBq) was 58 d, demonstrating moderate but significant improvement ($P = 0.002$).

In Vivo Toxicity and MTD. Mean body weight and urinalysis data after a single administration of 0.04- to 3.7-MBq doses are presented in Figure 7A. The MTD of ^{212}Pb-L2 in immunocompetent CD-1 mice was 1.5 MBq. Necropsy at 12 mo after treatment for lower doses (0.74 and 1.5 MBq) showed acceptable changes in hematologic parameters, including blood urea nitrogen (24–44 mg/dL) and creatinine (0.3 mg/dL) for kidney function and alanine aminotransferase and aspartate aminotransferase for liver function (Fig. 7B; Supplemental Tables 8–11). Relative kidney mass was comparable for both groups. Histopathologic evaluation revealed moderate nephrotoxicity and tubule epithelial karyomegaly in the treated compared with control animals (Fig. 7C), also chronic nephropathy with typical degenerative and regenerative changes that are expected in obese mice in chronic studies (*33*). No histopathologic radiotoxicity was noted in other organs, including bone marrow. Clinically evident toxicity of mice treated with 3.7 MBq was identified at 7 mo, including body weight loss, proteinuria, anemia, and azotemia in several animals. Those results support the dosimetry that designated kidney as the dose-limiting organ. The projection to human data is simplistic but indicates that activities on the order of 1–3 GBq could be delivered to humans, assuming MTD constraints of 23 Gy to the kidneys and 2 Gy to the bone marrow (Supplemental Table 7).

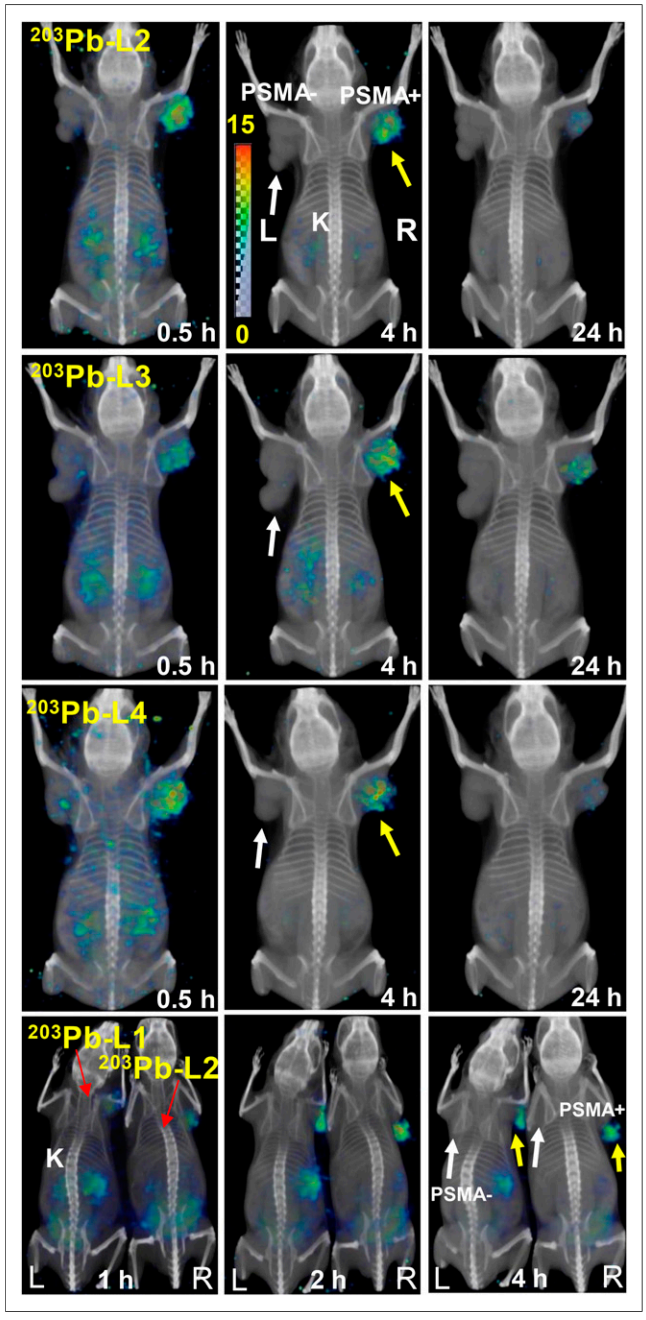

FIGURE 5. Whole-body volume-rendered SPECT/CT in mice bearing PSMA(+) PC3 PIP (yellow arrows) and PSMA(−) PC3 flu (white arrows) tumors. Mice were injected intravenously with ~26 MBq, showing uptake only in PSMA(+) PC3 PIP tumor and kidneys. K = kidney.

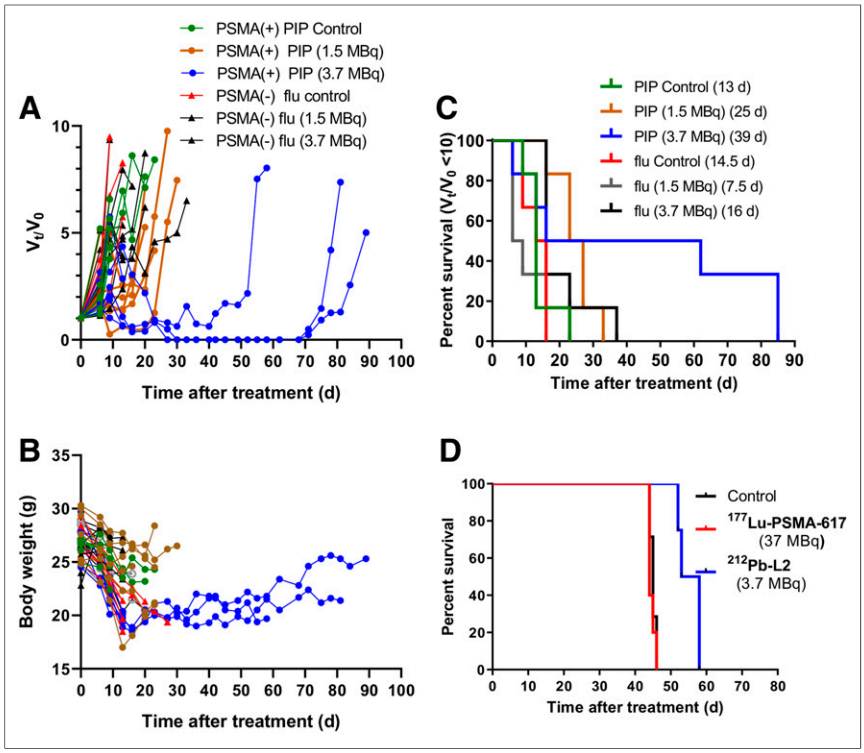

FIGURE 6. Treatment effect of ^{212}Pb-L2. (A) Ratio of tumor volume (tumor volume/initial volume) changes on treatment with single administration (n = 5). Each line represents 1 mouse. (B) Changes in body weight of the corresponding treatment group. Dose and median time for (tumor volume/initial volume) = 10 are in parentheses. (C) Kaplan–Meier curves illustrating time to grow 10-fold in tumor volume after treatment with a single administration of ^{212}Pb-L2 or control. (D) Kaplan–Meier curves showing significant improvement in survival after treatment in the micrometastatic model compared with control and ^{177}Lu-PSMA-617.

DISCUSSION

Although encouraging, PSMA-targeted ^{177}Lu-based β^--TRT is not effective in about 30% of patients and is considered unsuitable for patients with diffuse red marrow infiltration (*12*). ^{225}Ac-based α-TRT has been pursued to overcome resistance to β^--TRT as salvage therapy for treatment-refractory metastatic castration-resistant PC (*2*). Those clinical investigations have revealed that α-emitters are effective in controlling large lesions in addition to their predicted role in elimination of microscopic disease because of their short range of energy deposition and a noted bystander or abscopal effect. Several α-emitting isotopes, such as ^{213}Bi, ^{211}At, ^{212}Pb, and ^{225}Ac, have been studied clinically, and all are being investigated preclinically by us and others in the context of PSMA-based TRT (*15,16,19,20*).

There are several radiobiologic effects that contribute to the superior efficacy of α-emitters relative to β^--emitters, one of which is by activating several unique molecular pathways (*34*). That mechanism of radiotoxicity is independent of tissue oxygenation, dose rate, and cellular resistance to γ- or β^--irradiation and chemotherapy (*35*). Accordingly, normal tissues might also be expected to receive those higher toxic doses, causing severe side effects for the α- compared with β^--emitters. A careful evaluation of the absorbed doses from radiosensitive vital organs based on long-term toxicity studies as described in this report may provide reliable dose prediction for an initial phase I dose escalation trial.

The major acute toxicity from clinical PSMA-based α-TRT is related to salivary and lacrimal gland dysfunction (*5*). Although renal toxicity has so far proved minimal for PSMA β^-- and α-TRT (*2,12*), late nephrotoxicity remains a concern, as an insubstantial number of patients have been evaluated many years out from therapy. For example, over the long term, chronic nephrotoxicity was reported as a major side effect for patients treated with ^{177}Lu-/^{90}Y-octreotate (*36–38*). The α-emitters, because of their short-range radiation, may actually yield a lower absorbed dose to the radiosensitive glomeruli; however, they are much more potent with respect to promoting damage to the renal tubules (*39*). ^{225}Ac in particular, along with its 3 α-emitting daughters, is expected to have substantial radiotoxicity due to the redistribution of daughters to the normal organs after each α-decay. It is known that free bismuth is accumulated by the renal cortex (*39*), which is of concern because of the radioactive bismuth daughters of ^{225}Ac.

^{212}Pb offers an alternative for PSMA-based α-TRT because of its short half-life and its availability through a commercial generator. ^{212}Pb-based α-TRT using low-molecular-weight agents has not been studied extensively (*6*). The preclinical work described here leveraged several key features of the Lys-Glu-urea scaffold to optimize ^{212}Pb-based α-TRT targeting PSMA. An abbreviated structure–activity relationship study allowed us to modulate off-target toxicity while maintaining higher tumor-absorbed radiation dose. Because of the short half-life of ^{212}Pb, a high dose is expected to be delivered to the kidneys within the first few hours; consequently, we paid careful attention to the renal dose. Additionally, we anticipate a lower salivary gland absorbed dose for the ^{212}Pb-labeled compounds than for ^{225}Ac-labeled compounds because of the shorter half-life and less complicated dosimetry of ^{212}Pb. We recognize that direct comparison of salivary gland absorbed dose for ^{212}Pb- and ^{225}Ac-labeled analogs based on biodistribution data from ^{203}Pb-labeled compounds may be speculative since the studies were performed only out to 24 h after injection and the compounds harboring each radioisotope have their own pharmacokinetic properties.

Biodistribution data revealed that the agents with DOTA and DOTA-monoamide chelating agents (^{203}Pb-L1 and ^{203}Pb-L5) tended to display higher renal retention than the positively charged agents that carry TCMC as the chelator (^{203}Pb-L2–^{203}Pb-L4). Similarly, higher tumor uptake and retention were observed with ^{203}Pb-L1 and ^{203}Pb-L5 than with TCMC-chelated agents after 24 h. Among the TCMC-chelated compounds, ^{203}Pb-L2 without a 4-bromobenzyl moiety from the targeting lysine-urea-glutamate displayed significantly faster clearance from the PSMA(+) tumor and normal tissues at all time points. Although ^{203}Pb-L3 and ^{203}Pb-L4 demonstrated tumor uptake comparable to ^{203}Pb-L1 and ^{203}Pb-L5, they displayed significantly lower renal uptake at 4 h. However, the high tumor-to-kidney ratios of ^{203}Pb-L3 and ^{203}Pb-L4 were offset somewhat by their relatively high blood activity levels at early time-points compared with ^{203}Pb-L1 and ^{203}Pb-L5. Accordingly, ^{212}Pb-L2 was selected for the proof-of-concept α-TRT.

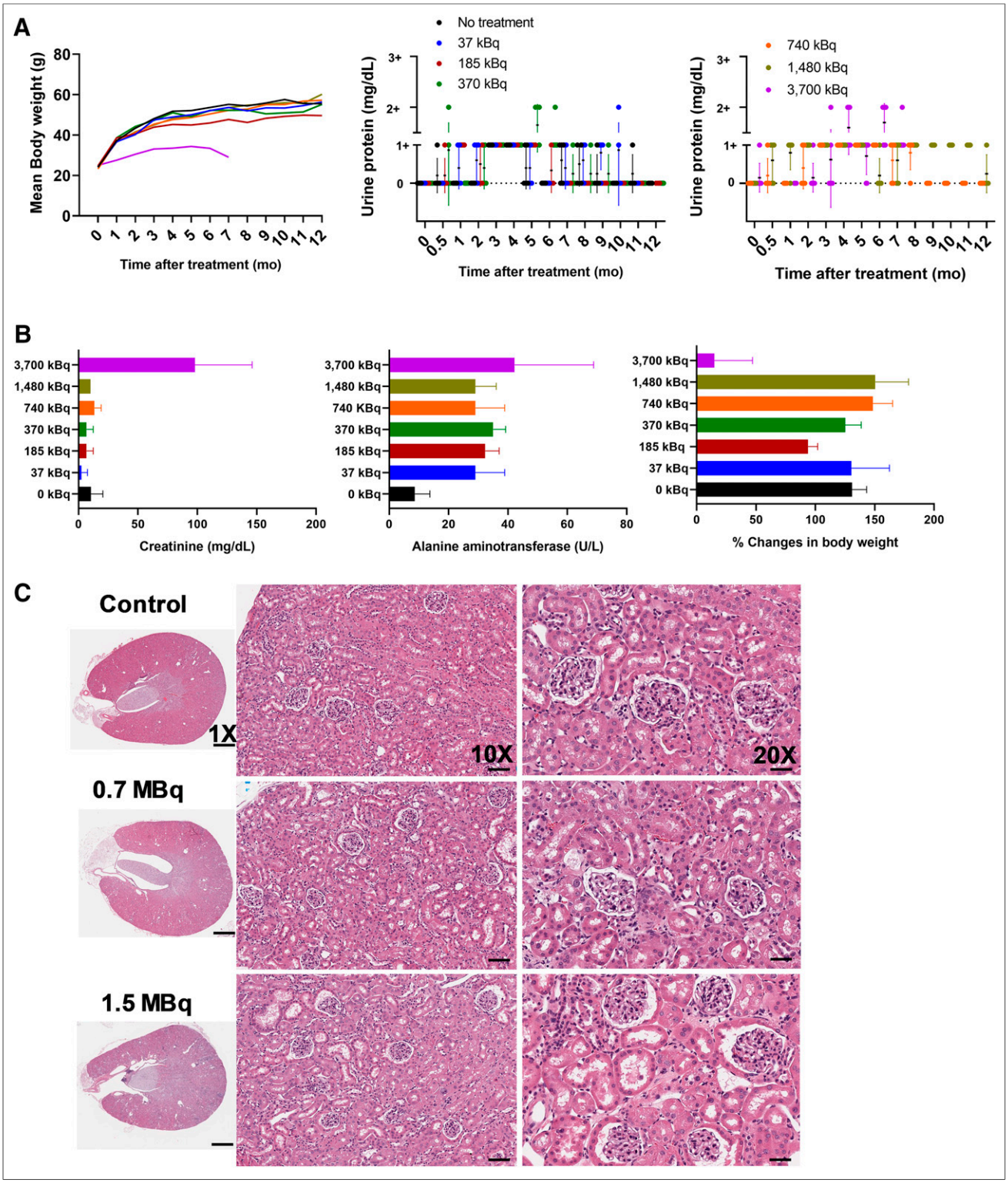

FIGURE 7. Analysis of radiotoxicity parameters after single administration of ^{212}Pb-L2 in healthy CD-1 mice (n = 5) for 1–12 mo. (A) Mean body weight and urine protein level measured by dipstick showing dose-dependent proteinuria occurring in the 3.7-MBq treatment group. A different batch of mice (n = 7) for treatment group was administered 3.7 MBq. Each dot represents the urine protein value for each mouse (trace, 0–10 mg/dL; 1+, 30 mg/dL; 2+,100 mg/dL). (B) Creatinine concentration and alanine aminotransferase in serum, and percentage body weight change at 13 mo after injection. All measurements for the 3.7-MBq treatment group were done at 7 mo after injection. (C) Hematoxylin and eosin staining of kidneys from nontreated mouse and mouse treated with 0.7 and 1.5 MBq of ^{212}Pb-L2 after 12 mo showing mild changes in cortical tubules (scale bar, 50 μm; ×20).

^{212}Pb-L2 significantly delayed growth of the PSMA(+) tumors. The median survival of animals receiving the agent was comparable to that for ^{211}At-6 (*15*). Significantly, ^{212}Pb-L2 demonstrated an approximately 6-fold lower kidney absorbed dose than our previous short-half-life α-emitting agent, ^{211}At-6 (*15*). Consequently, the MTD observed for a single administered dose in healthy, immunocompetent CD-1 mice increased from 37 kBq for ^{211}At-6 to 1.5 MBq for ^{212}Pb-L2. An administered dose of 3.7 MBq of ^{212}Pb-L2 showed characteristic features of late radiation nephropathy at 7 mo after treatment. In contrast, a dose of up to 1.5 MBq induced only discrete, nonspecific changes in the kidney while still enabling a measure of tumor growth control. To address the late nephropathy issue, we anticipate that a fractionated dose regimen would be more appropriate for this short-half-life radioligand. Alternatively, a partial kidney-blocking strategy using DCIBzL could be useful for ^{212}Pb-based α-TRT.

^{212}Pb-L2 also proved more effective in treating micrometastases than did β^--emitting ^{177}Lu-PSMA-617 in our PSMA(+) micrometastatic tumor model (*15*). That finding was most likely due to the superior capability of the high-linear-energy radiation of ^{212}Pb in this type of model and is consistent with previous reports using similar low-molecular-weight peptides and antibodies (*40–42*). Theoretically, the total energy for each ^{212}Pb disintegration is 6–8 MeV, compared with a mean β-radiation energy of 0.4 MeV for each ^{177}Lu disintegration—a 15-fold difference. The administered dose ratio for ^{212}Pb:^{177}Lu was 1:10, favored for ^{212}Pb-L2. A higher dose may be allowed for ^{212}Pb-L2 when considering a possible loss of activity after α-emission, and the half-life of ^{212}Pb-L2 (0.4 d) is much shorter than that of ^{177}Lu (6.7 d).

The high MTDs projected for humans as compared with other α-emitters can be explained by only 1 α-emission per ^{212}Pb decay, versus 4 for ^{225}Ac and ^{223}Ra; the shorter half-life; and the faster normal-organ biologic clearance. This explanation is also consistent with the murine MTD of 1.85–3.7 MBq, which is in the range of the fractional ^{223}Ra activity administered to humans. Nevertheless, such projections are highly uncertain, and any human application should be performed in increasing increments from values well below the calculated MTD.

Although ^{212}Pb-L2 displayed a short circulation time within blood and low renal uptake relative to other compounds in this series, long-term renal toxicity for the higher doses is a concern that is admittedly related to the physical characteristics of ^{212}Pb decay rather than to the in vivo stability of the ^{212}Pb-TCMC or ^{212}Pb-DOTA interactions. β-particle emission of ^{212}Pb is associated with γ-ray emission pathways that compete with internal conversion with 30% efficiency. Internal conversion decay destabilizes the resulting bismuth complexes, promoting rupture of the bichelator chemical bonds and resulting in release of ^{212}Bi, which is known to accumulate mainly in the renal proximal tubules (*11*). Therefore, the safety and efficacy of these new ^{212}Pb-based compounds could be further optimized with ex vivo murine studies and small-scale (macro-to-micro) dosimetry, with biokinetic modeling applied to clinical scenarios (*43*). An additional clinical consideration is that the ^{212}Pb decay chain includes several high-energy photons (1.6 MeV [1.5%]; 727 keV [6.6%]; 785 keV [1.1%]; 861 keV [4.5%]) that would possibly require hospitalization for radiation safety reasons.

CONCLUSION

We have evaluated in preclinical models the theranostic radionuclide pair ^{203}Pb/^{212}Pb in a focused series of compounds for PSMA-based α-TRT. ^{212}Pb-L2 demonstrated PSMA-specific tumor growth delay in both large and micrometastatic tumor models. The kidney was identified as the dose-limiting organ from the long-term toxicity study. Future studies are directed toward evaluation of the safety and efficacy of ^{212}Pb-L3–^{212}Pb-L5 studied at the MTD, in comparison with the corresponding long-lived α-emitters ^{225}Ac-L3–^{225}Ac-L5, as we work toward clinical translation with our optimized, lead compound.

DISCLOSURE

This work was supported by the Patrick C. Walsh Prostate Cancer Research Fund, P30CA006973, CA151838, CA134675, CA184228, CA183031, EB024495, and the Commonwealth Foundation. Drs. Banerjee, Minn, Mease, and Pomper are coinventors on one or more U.S. patents covering compounds discussed in this article and as such are entitled to a portion of any licensing fees and royalties generated by this technology. This arrangement has been reviewed and approved by the Johns Hopkins University in accordance with its conflict-of-interest policies. No other potential conflict of interest relevant to this article was reported.

KEY POINTS

QUESTION: Do PSMA-targeted α-emitting ^{212}Pb-labeled low-molecular-weight radioligands display the required safety and efficacy in preclinical studies for potential clinical translation as an alternative to long-half-life ^{225}Ac-based therapy with reduced off-target effects?

PERTINENT FINDINGS: Our report has addressed the question by examining strategic preclinical research. We generated 5 ^{212}Pb-labeled PSMA-targeted compounds and chose a lead among them, ^{212}Pb-L2, which demonstrated tumor growth control in both flank and micrometastatic models with the lowest off-target effects in this series. We determined the MTD of ^{212}Pb-L2 in healthy, immunocompetent mice to be 1.5 MBq to inform a future phase I clinical trial.

IMPLICATIONS FOR PATIENT CARE: ^{212}Pb-labeled α-emitters expand the possibilities for PSMA-targeted management of PC. The promising preclinical data, availability of commercial generators to produce ^{212}Pb, and relatively straightforward dosimetry, compared with other α-emitters, make Pb-labeled theranostic agents, including $^{203/212}$Pb-L2, attractive alternatives to existing TRT for PC.

REFERENCES

1. Parker C, Nilsson S, Heinrich D, et al. Alpha emitter radium-223 and survival in metastatic prostate cancer. *N Engl J Med.* 2013;369:213–223.
2. Kratochwil C, Bruchertseifer F, Rathke H, et al. Targeted alpha therapy of mCRPC with ^{225}actinium-PSMA-617: dosimetry estimate and empirical dose finding. *J Nucl Med.* 2017;58:1624–1631.
3. Zukotynski KA, Valliant J, Bénard F, et al. Flare on serial prostate-specific membrane antigen–targeted ^{18}F-DCFPyL PET/CT examinations in castration-resistant prostate cancer: first observations. *Clin Nucl Med.* 2018;43:213–216.
4. Afshar-Oromieh A, Debus N, Uhrig M, et al. Impact of long-term androgen deprivation therapy on PSMA ligand PET/CT in patients with castration-sensitive prostate cancer. *Eur J Nucl Med Mol Imaging.* 2018;45:2045–2054.
5. Langbein T, Chaussé G, Baum RP. Salivary gland toxicity of PSMA radioligand therapy: relevance and preventive strategies. *J Nucl Med.* 2018;59:1172–1173.
6. Miao Y, Hylarides M, Fisher DR, et al. Melanoma therapy via peptide-targeted α-radiation. *Clin Cancer Res.* 2005;11:5616–5621.
7. Milenic DE, Garmestani K, Brady ED, et al. Potentiation of high-LET radiation by gemcitabine: targeting HER2 with trastuzumab to treat disseminated peritoneal disease. *Clin Cancer Res.* 2007;13:1926–1935.

8. Meredith RF, Torgue J, Azure MT, et al. Pharmacokinetics and imaging of ^{212}Pb-TCMC-trastuzumab after intraperitoneal administration in ovarian cancer patients. *Cancer Biother Radiopharm.* 2014;29:12–17.
9. Meredith R, Torgue J, Shen S, et al. Dose escalation and dosimetry of first-in-human α radioimmunotherapy with ^{212}Pb-TCMC-trastuzumab. *J Nucl Med.* 2014;55: 1636–1642.
10. Atcher RW, Friedman AM, Hines JJ. An improved generator for the production of ^{212}Pb and ^{212}Bi from ^{224}Ra. *Int J Rad Appl Instrum [A].* 1988;39:283–286.
11. Yong K, Brechbiel MW. Towards translation of ^{212}Pb as a clinical therapeutic; getting the lead in! *Dalton Trans.* 2011;40:6068–6076.
12. Rahbar K, Ahmadzadehfar H, Kratochwil C, et al. German multicenter study investigating ^{177}Lu-PSMA-617 radioligand therapy in advanced prostate cancer patients. *J Nucl Med.* 2017;58:85–90.
13. Hofman MS, Violet J, Hicks RJ, et al. ^{177}Lu-PSMA-617 radionuclide treatment in patients with metastatic castration-resistant prostate cancer (LuPSMA trial): a single-centre, single-arm, phase 2 study. *Lancet Oncol.* 2018;19:825–833.
14. McDevitt MR, Barendswaard E, Ma D, et al. An alpha-particle emitting antibody ([^{213}Bi]J591) for radioimmunotherapy of prostate cancer. *Cancer Res.* 2000;60:6095–6100.
15. Kiess AP, Minn I, Vaidyanathan G, et al. (2*S*)-2-(3-(1-carboxy-5-(4-^{211}At-astatobenzamido)pentyl)ureido)-pentanedioic acid for PSMA-targeted alpha-particle radiopharmaceutical therapy. *J Nucl Med.* 2016;57:1569–1575.
16. Kelly JM, Amor-Coarasa A, Ponnala S, et al. A single dose of ^{225}Ac-RPS-074 induces a complete tumor response in an lncap xenograft model. *J Nucl Med.* 2019;60:649–655.
17. Nonnekens J, Chatalic KL, Molkenboer-Kuenen JD, et al. ^{213}Bi-labeled prostate-specific membrane antigen-targeting agents induce DNA double-strand breaks in prostate cancer xenografts. *Cancer Biother Radiopharm.* 2017;32:67–73.
18. Miao Y, Figueroa SD, Fisher DR, et al. Lead-203-labeled alpha-melanocyte stimulating hormone peptide as an imaging probe for melanoma detection. *J Nucl Med.* 2008;49:823–829.
19. Ray S, Kumar V, Lisok A, et al. Low and high LET radiometal-based therapeutics for prostate cancer [abstract]. *J Nucl Med.* 2017;58(suppl):312.
20. Dos Santos JC, Schäfer M, Bauder-Wüst U, et al. Development and dosimetry of ^{203}Pb/^{212}Pb-labelled PSMA ligands: bringing "the lead" into PSMA-targeted alpha therapy? *Eur J Nucl Med Mol Imaging.* 2019;46:1081–1091.
21. Banerjee SR, Foss CA, Pullambhatla M, et al. Preclinical evaluation of ^{86}Y-labeled inhibitors of prostate-specific membrane antigen for dosimetry estimates. *J Nucl Med.* 2015;56:628–634.
22. Chen Y, Foss CA, Byun Y, et al. Radiohalogenated prostate-specific membrane antigen (PSMA)-based ureas as imaging agents for prostate cancer. *J Med Chem.* 2008;51:7933–7943.
23. Garmestani K, Milenic DE, Brady ED, Plascjak PS, Brechbiel MW. Purification of cyclotron-produced ^{203}Pb for labeling Herceptin. *Nucl Med Biol.* 2005;32:301–305.
24. Banerjee SR, Pullambhatla M, Byun Y, et al. Sequential SPECT and optical imaging of experimental models of prostate cancer with a dual modality inhibitor of the prostate-specific membrane antigen. *Angew Chem Int Ed Engl.* 2011;50:9167–9170.
25. Banerjee SR, Kumar V, Lisok A, et al. ^{177}Lu-labeled low-molecular-weight agents for PSMA-targeted radiopharmaceutical therapy. *Eur J Nucl Med Mol Imaging.* August 10, 2019 [Epub ahead of print].
26. Tykvart J, Schimer J, Barinkova J, et al. Rational design of urea-based glutamate carboxypeptidase II (GCPII) inhibitors as versatile tools for specific drug targeting and delivery. *Bioorg Med Chem.* 2014;22:4099–4108.
27. Baidoo KE, Milenic DE, Brechbiel MW. Methodology for labeling proteins and peptides with lead-212 (^{212}Pb). *Nucl Med Biol.* 2013;40:592–599.
28. Yamamoto T, Saito O, Aoe T, et al. Local administration of N-acetylaspartylglutamate (NAAG) peptidase inhibitors is analgesic in peripheral pain in rats. *Eur J Neurosci.* 2007;25:147–158.
29. Bolch WE, Eckerman KF, Sgouros G, Thomas SR. MIRD pamphlet no. 21: a generalized schema for radiopharmaceutical dosimetry—standardization of nomenclature. *J Nucl Med.* 2009;50:477–484.
30. Stabin MG, Sparks RB, Crowe E. OLINDA/EXM: the second-generation personal computer software for internal dose assessment in nuclear medicine. *J Nucl Med.* 2005;46:1023–1027.
31. Chappell LL, Dadachova E, Milenic DE, Garmestani K, Wu C, Brechbiel MW. Synthesis, characterization, and evaluation of a novel bifunctional chelating agent for the lead isotopes ^{203}Pb and ^{212}Pb. *Nucl Med Biol.* 2000;27:93–100.
32. Ray Banerjee S, Pullambhatla M, Foss CA, et al. Effect of chelators on the pharmacokinetics of ^{99m}Tc-labeled imaging agents for the prostate-specific membrane antigen (PSMA). *J Med Chem.* 2013;56:6108–6121.
33. Kidney. National Toxicology Program website. https://ntp.niehs.nih.gov/nnl/urinary/kidney/index.htm. Updated October 23, 2014, Accessed August 20, 2019.
34. Baidoo KE, Yong K, Brechbiel MW. Molecular pathways: targeted α-particle radiation therapy. *Clin Cancer Res.* 2013;19:530–537.
35. Sgouros GE. *MIRD Monograph: Radiobiology and Dosimetry for Radiopharmaceutical Therapy with Alpha-Particle Emitters.* Reston, VA: Society of Nuclear Medicine and Molecular Imaging; 2015.
36. Bodei L, Kidd M, Paganelli G, et al. Long-term tolerability of PRRT in 807 patients with neuroendocrine tumours: the value and limitations of clinical factors. *Eur J Nucl Med Mol Imaging.* 2015;42:5–19.
37. Gabriel M, Nilica B, Kaiser B, Virgolini IJ. Twelve-year follow-up after peptide receptor radionuclide therapy (PRRT). *J Nucl Med.* 2019;60:524–529.
38. Bergsma H, Konijnenberg MW, van der Zwan WA, et al. Nephrotoxicity after PRRT with ^{177}Lu-DOTA-octreotate. *Eur J Nucl Med Mol Imaging.* 2016;43:1802–1811.
39. Miederer M, McDevitt MR, Sgouros G, Kramer K, Cheung N-KV, Scheinberg DA. Pharmacokinetics, dosimetry, and toxicity of the targetable atomic generator, ^{225}Ac-hum195, in nonhuman primates. *J Nucl Med.* 2004;45:129–137.
40. Wild D, Frischknecht M, Zhang H, et al. Alpha- versus beta-particle radiopeptide therapy in a human prostate cancer model (^{213}Bi-DOTA-PESIN and ^{213}Bi-AMBA versus ^{177}Lu-DOTA-PESIN). *Cancer Res.* 2011;71:1009–1018.
41. Miederer M, Henriksen G, Alke A, et al. Preclinical evaluation of the alpha-particle generator nuclide ^{225}Ac for somatostatin receptor radiotherapy of neuroendocrine tumors. *Clin Cancer Res.* 2008;14:3555–3561.
42. Song H, Hobbs RF, Vajravelu R, et al. Radioimmunotherapy of breast cancer metastases with alpha-particle emitter ^{225}Ac: comparing efficacy with ^{213}Bi and ^{90}Y. *Cancer Res.* 2009;69:8941–8948.
43. Hobbs RF, Song H, Huso DL, Sundel MH, Sgouros G. A nephron-based model of the kidneys for macro-to-micro alpha-particle dosimetry. *Phys Med Biol.* 2012;57:4403–4424.